PAPER
Nadine Borduas-Dedekind *et al.*
Singlet oxygen is produced from brown carbon-containing
cooking organic aerosols (BrCOA) under indoor lighting

Check for updates

Singlet oxygen is produced from brown carbon-containing cooking organic aerosols (BrCOA) under indoor lighting†

Nadine Borduas-Dedekind, [ID] *[a] Keighan J. Gemmell, [ID] [a] Madushika Madri Jayakody,[a] Rickey J. M. Lee, [ID] [a] Claudia Sardena [ID] [a] and Sebastian Zala[b]

Light absorbing organic molecules known as brown carbon (BrC) can be emitted during processes such as cooking and combustion in indoor environments. We hypothesized that indoor BrC-containing cooking organic aerosols, or BrCOA, can act as sensitizers to generate the first excited state of molecular oxygen, singlet oxygen ($^1O_2^*$), under indoor lighting conditions. Here, we used an impinger to collect aerosols from a range of cooking dishes, including pancakes, pan-fried Brussels sprouts and vegetable stir-fries, and irradiated these samples in a photoreactor with UVA and fluorescent lights and on a sunlit windowsill. Using furfuryl alcohol as a probe for $^1O_2^*$, we determined steady-state concentrations of $^1O_2^*$ using liquid chromatography and calculated apparent quantum yields for each BrCOA sample. Our results show that under all indoor lighting conditions tested, BrCOA can indeed sensitize $^1O_2^*$. Specifically, in solutions of BrCOA from pancakes, pan-fried Brussels sprouts, and vegetable stir-fries under UVA light, the $^1O_2^*$ concentrations were $2.56 \pm 1.24 \times 10^{-13}$ M, $2.24 \pm 1.51 \times 10^{-13}$ M, and $3.12 \pm 0.86 \times 10^{-13}$ M, respectively. These results suggest that $^1O_2^*$ production is not dish-dependent, but rather produced across a range of BrCOA samples. We then normalized the $^1O_2^*$ concentrations to the rate of absorbance to obtain apparent quantum yields up to 6.1%. Both the quality and the quantity of the chromophoric BrCOA were important for predicting the apparent quantum yield. Moreover, the indoor sunlit experiments led to the highest $^1O_2^*$ concentrations observed, with important implications on the formation of oxidants in sunlit kitchens. These results demonstrate the ability of BrCOA to produce $^1O_2^*$ in indoor environments, and thus for $^1O_2^*$ to be a competitive indoor oxidant.

Environmental significance

With the growing appreciation that indoor light can initiate photochemical processes, we hypothesized that brown carbon-containing cooking organic aerosols, or BrCOA, could sensitize the first excited state of molecular oxygen: singlet oxygen ($^1O_2^*$). Here, we show that BrCOA from pancakes, pan-fried Brussels sprouts and vegetable stir-fries can efficiently produce $^1O_2^*$ under the irradiation of UVA, fluorescent bulbs and a sunlit windowsill. We observed a sustained production of $^1O_2^*$ under all light sources, indicating that $^1O_2^*$ can be a competitive oxidant in indoor environments and has the prolonged ability to oxidize indoor aerosols and impact air quality.

1 Introduction

Brown carbon (BrC) is the component of organic aerosol which absorbs in the near ultraviolet (UV) region of the visible spectra.[1,2] BrC can originate from incomplete combustion processes outdoors and indoors. Cooking organic aerosols (COA) are a major source of BrC emissions indoors,[3,4] and contribute to urban outdoor organic aerosols.[5–7] In fact, recent studies suggest that residential cooking contributes more to urban pollution than traffic emissions.[8,9] According to Zhu *et al.*,[10] residential combustion accounts for 60% of total surface BrC concentrations in China. Furthermore, Sankhyan *et al.*[3] reported BrC concentrations up to 10 times higher during cooking activities in the HOMEChem study.[11]

When exposed to light, chromophoric species contained in BrC can act as photo-sensitizers, generating reactive oxygen species (ROS) *via* the formation of triplet state organics.[12–17] Singlet oxygen ($^1O_2^*$) is a ROS and is the first excited state of molecular oxygen (O_2), produced by indirect photochemistry.[18]

[a]*Department of Chemistry, University of British Columbia, Vancouver, V6T 1Z1, Canada. E-mail: borduas@chem.ubc.ca; Tel: +1 604 822 4435*

[b]*Department of Environmental Science Systems, ETH Zürich, Zürich, 8092, Switzerland*

© 2024 The Author(s). Published by the Royal Society of Chemistry

Environ. Sci.: Atmos., 2024, 4, 611–619 | 611

Faust and Allen[19] reported the first measurements of $^1O_2^*$ steady state concentrations ($[^1O_2^*]_{ss}$) in cloud water, 2.7–110×10^{-13} M. Subsequently, fog water, cloud water and aqueous solutions of ambient particulate matter have been shown to produce $^1O_2^*$ under laboratory irradiated conditions.[20–27]

Unlike the outdoor environment, indoor spaces do not receive full spectrum sunlight (290 nm to 800 nm), as most of the shorter wavelengths (<320 nm) are attenuated by windows.[28,29] Historically, the oxidative capacity of the indoor environment has been thought to be governed by non-photolytic reactions and instead by physical transport of oxidants such as ozone from outdoors.[29] However, there is growing evidence that high-enough energy photons are indeed available indoors to initiate indoor photochemistry.[28,30] Kowal et al.[31] showed that direct and indirect sunlight from the windows and fluorescent tubes can initiate indoor photolysis of nitrous acid (HONO) and formaldehyde (HCHO) leading to the formation of OH radicals and HO_2 radicals. HONO has also been observed to be formed indoors from photochemistry on glass windows.[32] In addition, OH radicals have been detected in concentrations up to 1.8×10^6 molecules per cm^3 in a sunlit classroom where indoor solar irradiation with wavelengths as low as 320 nm penetrated through glass windows.[33]

Combining this recent evidence of indoor photochemistry and the ability of cooking to form BrC, we considered the ability of brown carbon-containing cooking organic aerosols (BrCOA) to initiate photochemical species such as triplet state organics and subsequently $^1O_2^*$. We hypothesized that BrCOA could act as sensitizers to generate $^1O_2^*$ under indoor lighting conditions.

In this study, we report the first measurements of $^1O_2^*$ from BrCOA produced under indoor light. We selected 3 types of dishes to represent a range of pan-cooking events and to produce diverse COA representative of breakfast, lunch and dinner. First, pancake experiments were chosen to represent exposure to indoor BrC during breakfast. Next, pan-fried Brussels sprouts were chosen based on the HOMEChem study where Brussels sprouts were part of the Thanksgiving dinner and generated high concentrations of BrC and COA.[34,35] Finally, we chose the vegetable stir-fry following the work by Patel et al.[34] identifying this dish as producing high amounts of large particles, including PM_{20}. In addition, Davies et al.[36] have recently demonstrated that VOC emissions from stir-fry are dominated by alcohols and contain aldehydes and terpenes from heating of oil and spices, potentially acting as chromophoric species in BrCOA. We collected the water-soluble portion of the BrCOA using an impinger and irradiated the filtered solutions under UVA, fluorescent and sun-light through a window to represent a range of indoor light conditions within a home kitchen. We found that all types of dishes and lights effectively produced $^1O_2^*$ with implications for indoor air quality.

2 Methods

2.1 Chemicals

Furfuryl alcohol (FFA, Sigma-Aldrich, 98%) was distilled under reduced pressure to a colourless liquid according to Armarego and Chai[37] and stored under N_2 in the fridge. para-

Nitroanisole (Millipore-Sigma, 97%) was recrystallized in petroleum ether.[37] Perinaphthenone (97%), pyridine (≥99.9%), and 2-propanol (HPLC grade, ≥99.9%) were purchased from Millipore-Sigma and used as is. All solutions were prepared using 18.2 MΩ cm Milli-Q water (ELGA Lab-water, Purelab Option-Q model).

2.2 Experimental cooking setup

Cooking aerosol sampling experiments took place in the laboratory (Fig. S1†). A cooking plate, a pan and a spatula were used to cook the dishes. Foodstuff was bought at the local grocery store. The dishes included pancakes, Brussels sprouts, and vegetable stir-fries (see the ESI† for the list of ingredients and the recipes).

Before, during and after the experiments, a scanning mobility particle sizer (SMPS) (Model 3082. TSI Inc.), an optical particle sizer (OPS 3330, TSI Inc.) were used to measure COA. A Coriolis μ impinger (Bertin Technologies, France) was used to collect the ambient and cooking aerosols (Fig. S1†). Prior to sampling COA, background lab air was sampled for 60 min using the Coriolis impinger, and subsequently the COA were also sampled for 60 min.

2.2.1 Ambient aerosol mass concentrations. The SMPS is composed of an electrostatic classifier (model 3082), a differential mobility analyzer (DMA, model 3088) and a butanol condensation particle counter (Model 3750. TSI Inc.) connected by a 25.4 cm tubing (TSI conductive silicone tubing). The DMA was operated using an impactor (0.0508 cm), an aerosol inlet flow rate of 1 L min^{-1} and a sheath flow rate of 10 L min^{-1} to measure particles in the size range of 8.4 to 294 nm. The scan time was 46 s, with a 10 s purge time and a total run time of 1 min. Multiple charge and diffusion corrections were enabled. The OPS was operated with an inlet flow rate of 1 L min^{-1}, a total run time of 1 min and a size range of 327 nm to 9.02 μm. The inlet of the aerosol instruments were 1 m-long TSI conductive silicone tubing and co-located with the Coriolis μ
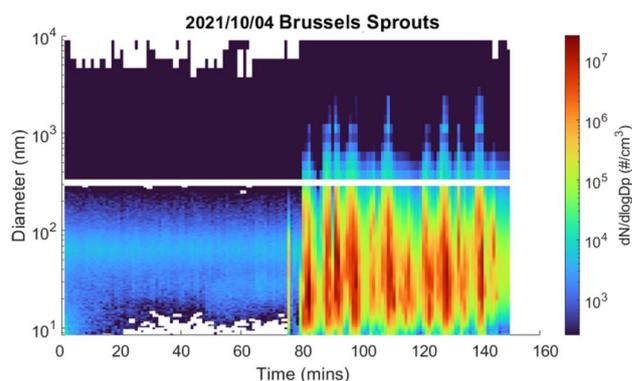

Fig. 1 The number concentration and diameter of COA produced during 1 h of pan-frying Brussels sprouts following a 1 h ambient background aerosol measurement. The lower size range was measured by the SMPS and the larger size range was measured by the OPS. The cooking evidently started at 75 min. Recipes and ingredients are in the ESI.†

612 | Environ. Sci.: Atmos., 2024, 4, 611–619

© 2024 The Author(s). Published by the Royal Society of Chemistry

impinger inlet (Fig. S1†). The increase in COA was clearly evident during the cooking events (Fig. 1 & S10†).

2.2.2 Aerosol impinger collection. Indoor aerosols were directly collected into Milli-Q water using a Coriolis μ impinger. This instrument is designed for outdoor bio-aerosols sampling such as pollen and spores,[38] but can also be used in aerosol sampling with the benefit of avoiding a filter extraction step.[39] Consequently, our samples are not extracts as they were not collected on filters, were not solvent-extracted, and thus do not suffer from extraction artifacts.[40]

Prior to the measurement, the Coriolis μ impinger, the inlet and the sampling cones were autoclaved and washed with Milli-Q water. 15 mL of Milli-Q water was added to the sampling cone as the collection liquid and the Coriolis was programmed for 10 min. The collection cone was refilled to 15 mL every 10 min. During the collection, air was drawn into the cone at a flow rate of 300 L min^{-1}, creating a vortex inside the sampling cone and allowing the larger particles and the water-soluble components to be captured within the aqueous solution.[39] This technique does have its limitations however, as the particle collection efficiency drops below 0.5 μm.[38]

Collected COA were subsequently diluted into 50 mL and filtered through 0.22 μM, 33 mm, PES-GP sterile syringe filters. Filtering was necessary to remove oil from the COA and suspended particulates, as the presence of the oil and particulates prevented homogeneous light exposure in our setup. Our samples therefore represent a subset of BrCOA and hence a lower bound of the potential photochemistry investigated. The background aerosol solutions were clear and colorless. Filtered COA and background samples were stored in the refrigerator at 4 °C in 40 mL amber vials.

2.2.3 Calculating total mass using SMPS and OPS data. We used the SMPS and OPS particle size distributions to estimate the total COA mass of the particles per unit volume of air sampled in μg m^{-3} collected by the Coriolis impinger. This calculation represents an upper bound of the organic material in solution as the collection efficiency of the Coriolis impinger drops for particles below 0.5 μm.[38] The density of the cooking aerosol samples was assumed to be 1 g cm^{-3} following the recommendation by Katz et al.[40] The detailed calculations of the SMPS and OPS mass concentrations (μg m^{-3}) to estimate the mass collected in the Coriolis are further detailed in the ESI.†

2.3 UV/Vis measurements

To characterise the chromophores within the COA solutions, we measured the absorbance of the filtered samples using a UV/Vis spectrometer (Carry-5000, Agilent). A baseline correction with filtered Milli-Q water was applied to all the measurements. Furthermore, we ensured that the absorbance of all samples reached zero at 800 nm and integrated our data for apparent quantum yield calculations up to 800 nm as recommended in Ossola et al.[18]

2.4 Irradiation experiments

2.4.1 Photoreactor. Photochemical experiments were performed using a photoreactor (Rayonet, Model RPR-200, The Southern New England Ultraviolet Co.). The Rayonet was equipped with either twelve 365 nm UVA light or twelve fluorescent tube bulbs (Philips, 3000 K) to mimic indoor lighting conditions (Fig. 2). During an experiment, borosilicate test tubes were placed in a rotating carousel. All slots were occupied by tubes containing either a BrCOA extract or water to ensure that the light path was even throughout the experiment. The temperature was controlled using a fan underneath the carousel and the temperature was measured using an IR thermometer (Commercial Electric, MS6520H) to be 30 °C throughout the experiment. Absolute irradiance of the photoreactor was determined by an Ocean Optics FLAME-T-UV-VIS spectrophotometer (QP600-1-XSR fiber optic and CC-3-UV-S cosine receptor) (Fig. 2). The irradiance inside the borosilicate test tubes was determined by using the *para*-nitroanisole/pyridine chemical actinometer as described in Laszakovits et al.[41] and in Borduas-Dedekind et al.[42] (see Section 2.7).

2.4.2 Sunlight. A subset of COA solutions were also exposed to sunlight through a south-facing window in the spring of 2022 in Vancouver, British Columbia (Fig. S2†). These experiments were particularly weather dependent and not all samples were able to undergo this sunlit exposure. These sunlit experiments were conducted over a few hours, yet despite a change in irradiance, the furfuryl alcohol probe decay remained linear indicating steady-state conditions (Fig. S6†). In an effort to normalize the sunlight irradiation, we simulated a solar spectrum (global horizontal irradiance, 300–400 nm, with an integrated irradiance of 59.2 J s^{-1} m^{-2}) using the SMARTS 2.9.5 (NREL) model. The simulated measurement location and time is a generic point at mid-latitudes (45°) in summer (1 June, from 05:00 a.m. to 07:00 p.m.).[42]

2.5 Quantification of $^1O_2^*$ steady-state concentrations

2.5.1 FFA decay measured by HPLC. Furfuryl alcohol (FFA) was used as the chemical probe to calculate steady state concentrations and apparent quantum yields of $^1O_2^*$.[43,44] For an irradiation experiment, the sample solution was added to a borosilicate test tube with 50 μM of FFA and 10 μM of isopropanol. The isopropanol was used as an OH radical scavenger to ensure that the FFA decay is solely due to reactivity with $^1O_2^*$.[24]

To monitor the decay of FFA as a function of illumination, 75 μL aliquots were sampled at different time points and analyzed by high performance liquid chromatography (HPLC, Agilent technologies, USA) coupled with a diode array detector (DAD). The HPLC was equipped with a reverse phase C18 column (5 μm; 4.6 × 150 mm) and a photodiode array detector (G4212B 1260 DAD). Using the DAD detector, maximum absorbance of FFA was measured at 219 nm.[43] The flow rate was set to 1 mL min^{-1}, and the gradient method included 3 min at 75/25 (water/ACN), 3 min at 50/50, 2 min at 25/75 (water/ACN), and 2 min at 100% water, for a total run duration of 10 min. FFA was monitored at 219 nm (ref. 24) and observed at a retention time of 1.57 min.

2.5.2 $^1O_2^*$ steady-state concentration calculation. $^1O_2^*$ steady state concentrations can be calculated by using pseudo-first order rate kinetics of the FFA probe.[18,44] The second order rate constant of the reaction of FFA with $^1O_2^*$ is well constrained

© 2024 The Author(s). Published by the Royal Society of Chemistry

Environ. Sci.: Atmos., 2024, **4**, 611–619 | **613**

and has the following temperature dependence: k_{FFA} [L mol^{-1} s^{-1}] = $1 \times 10^8 + 2.1 \times 10^6(T[°C] - 22)$.[44] The temperature of the photoreactor in our experimental set up was 30 °C, and we therefore used the temperature-corrected FFA rate constant of 1.19×10^8 M^{-1} s^{-1} for the UVA and the fluorescent lights experiments. For the sunlight experiment, we used the FFA rate constant of 1.00×10^8 M^{-1} s^{-1} at 22 °C.

From the obtained HPLC chromatograms, we monitored the decay of FFA over irradiation time. We then plotted the natural log of this decay, $\ln([FFA]_t/[FFA]_0)$ as a function of time to obtain k_{obs} following eqn (1), and subsequently divided k_{obs} by the temperature-dependent FFA rate constant k_{FFA} to obtain the $[^1O_2^*]_{ss}$ from eqn (2).

$$\ln\left(\frac{[FFA]_t}{[FFA]_0}\right) = k_{obs} \times t \tag{1}$$

$$[^1O_2^*]_{ss} = \frac{k_{obs}}{k_{FFA}} \tag{2}$$

The effectiveness of FFA as a probe for $^1O_2^*$ relies on its pseudo-first order kinetics. We observed that experiments with longer exposure times, and thus lower $^1O_2^*$ production, sometimes deviated from pseudo-first order kinetics. In particular, experiments with fluorescent tubes resulted in non-linear regressions at longer irradiation, indicating that these time points were no longer experiencing steady-state concentrations of $^1O_2^*$ (Fig. S5†). We addressed this issue by determining the percentage change in slope by removing the later time points which deviated from pseudo-first order kinetics. A change in slope greater than 25% led to the removal of these points (see top panels of Fig. S4–S6† for all raw data, and bottom panels for the adjusted linear regressions).

2.5.3 Control experiments. Control experiments were performed to further ensure that the decay of the FFA probe was due solely to its reactivity with $^1O_2^*$. Dark controls were performed using 50 μM FFA and covering the test tube with aluminium foil. No decay was observed, confirming the photochemical requirement for these reactions to proceed. All COA had a corresponding background ambient air sample which was also run with 50 μM FFA and 10 μM of isopropanol. The background ambient air samples showed no quantifiable FFA decay, indicating that the reactivity was due to BrCOA (Fig. S7†).

2.6 Relative probe based method for apparent quantum yield calculations

2.6.1 Perinaphthenone as a reference sensitizer. We use the apparent quantum yield nomenclature here since the specific sensitizer producing $^1O_2^*$ is not known, and instead BrCOA is a complex mixture of chromophores. We quantified apparent $^1O_2^*$ quantum yields using perinapthenone (PN) as a reference sensitizer.[18,45] A solution of 50 μM of FFA, 10 μM of isopropanol and 10 μM of perinapthenone (PN) was used as the reference sensitizer solution for each irradiation experiments. The solution with perinapthenone was irradiated for only 8 minutes, due to its high

quantum yield, and time points were taken throughout the irradiation. FFA decays due to its reaction with perinapthenone for all experiments conducted are shown in Fig. S8†.

2.6.2 Apparent quantum yield calculation. Perinapthenone is a highly efficient $^1O_2^*$ sensitizer with a wavelength-independent quantum yield of 1.[18] As $^1O_2^*$ is in steady state conditions for all sensitizers, including our reference sensitizer, apparent $^1O_2^*$ quantum yields can be calculated as:

$$\Phi_{^1O_2} = \frac{k_{obs}^{sample}}{R_{abs}^{sample}} \times \frac{R_{abs}^{PN}}{k_{obs}^{PN}} \times \Phi_{PN} \tag{3}$$

where k_{obs} is the pseudo-first-order degradation rate constant of FFA, PN is perinapthenone, and R_{abs} is defined as:

$$R_{abs} = 2.303 \sum_\lambda (I_{\lambda,m} \times abs_\lambda \times sf_\lambda) \tag{4}$$

where $I_{\lambda,m}$ is the spectral irradiance of the source light; abs_λ is the spectral absorbance of the sample obtained from UV/Vis spectroscopy; sf_λ is the screening factor defined as $\frac{1 - 10^{abs_\lambda}}{2.3 \times abs_\lambda}$.[23]

2.7 Chemical actinometry

2.7.1 Experimental details. Chemical actinometry experiments were conducted to quantify the light intensity inside the test tube and to normalize the irradiation time for each light source.[23,24,41,42] We chose to normalize to UVA bulbs as they produced the largest rates of absorbance with the BrCOA.

A solution containing 20 μM of recrystallized *para*-nitroanisole and 0.25 mM pyridine in Milli-Q water was irradiated for 5 h in the photoreactor.[41] Samples were taken at different irradiation time points, and *para*-nitroanisole was quantified using high pressure liquid chromatography (HPLC) equipped with a reverse phase C18 column (5 μm; 4.6 × 150 mm) and a photodiode array detector (G4212B 1260 DAD). Analyses were performed using the isocratic mode and a 50/50 eluent of acetonitrile and 90% acetate butter (pH = 6) in 10% acetonitrile. The flow rate was set to 1 mL min^{-1} and the sample injection volume was 20 μL. Under these conditions, *para*-nitroanisole eluted at 3.8 min and was detected at 316 nm. The pseudo first-order decay rate for *para*-nitroanisole ($k_{deg,PNA}$) was determined to be $7.73 \pm 0.44 \times 10^{-5}$ s^{-1} for UVA and $5.86 \pm 0.65 \times 10^{-6}$ s^{-1} for fluorescent lights. Errors are reported as the standard deviation of triplicate experiments shown in Fig. S9†.

2.7.2 Absolute irradiance calculation. In addition to reporting R_{abs} and using this value for the apparent quantum yield calculation, we also calculated the absolute spectral irradiance, $I_{\lambda,0}$, according to Laszakovits et al.[41]

$$I_{\lambda,0} = s \times I_{\lambda,m} \tag{5}$$

where s is the wavelength independent scaling factor, defined as:

$$s = \frac{k_{deg,PNA} \times [PNA]_0 \times l}{\Phi_{deg,PNA} \times \sum_\lambda (I_{\lambda,m} \times f_{\lambda,PNA} \times \Delta\lambda)} \tag{6}$$

where PNA is *para*-nitroanisole, and where $f_{\lambda,PNA}$ is:

$$f_{\lambda,\text{PNA}} = 1 - 10^{-\varepsilon_{\lambda,\text{PNA}} \times [\text{PNA}]_0 \times l} \tag{7}$$

Based on the $k_{\text{deg,PNA}}$ values and the spectral irradiance measurements for UVA and fluorescent light obtained by the spectrophotometer, we calculated the absolute spectral irradiance (integrated for 280–400 nm) of these photochemistry setups as $I_{\lambda,0} = 222.45 \pm 10$ W m^2 and $I_{\lambda,0} = 11.25 \pm 3.96$ W m^2, respectively. In order to compare the irradiance sources, we determined a conversion factor from the irradiation time in the photoreactor into the equivalent irradiation time in sunlight and fluorescent.[42]

We report R_{abs} in mol$_{\text{photons}}$ L^{-1} s^{-1} nm^{-1} for apparent quantum yield calculations, but we report absolute irradiance in W m^{-2} nm^{-1} and converted to mmol$_{\text{photons}}$ cm^{-2} s^{-1} nm^{-1} as below.[18]

$$I_{\lambda,\text{mm}} = \frac{I_{\lambda,\text{m}}\lambda}{hcN_{\text{A}}} \times 10^{-10} \tag{8}$$

where $I_{\lambda,\text{m}}$ is the irradiance measured by the FLAME spectrometer with units of W m^{-2} nm^{-1}, $I_{\lambda,\text{mm}}$ is the irradiance with units of mmol$_{\text{photons}}$ cm^{-2} s^{-1} nm^{-1}, λ is the respective wavelength at which the spectral irradiance is calculated, c is the speed of light, h is the Planck constant (6.626×10^{-34} J s), N_{A} is the Avogadro number (6.023×10^{23} mol^{-1}), and 10^{-10} is the m^2 to cm^2 and mol to mmol unit conversion.

2.7.3 Actinometry conversion factors. The conversion factor represents the irradiation time of 1 h of sunlight and of 1 h of fluorescent bulbs equivalent to the irradiation in the Rayonet with UVA bulbs.

$$\text{Fluorescent conversion factor} = \frac{R_{\text{abs,fluorescent}}}{R_{\text{abs,UVA}}} \tag{9}$$

$$\text{Sun conversion factor} = \frac{R_{\text{abs,sun}}}{R_{\text{abs,UVA}}} \tag{10}$$

where R_{abs} is defined as eqn (4) for each irradiation source. Conversion factors for each BrCOA sample are reported in Table S1.† Since the variability of the conversion factors is small between dish types, we can average these values, leading to an average conversion factor for 1 h of fluorescent light to 0.07 h of UVA exposure, and for 1 h of indoor sunlight to 0.37 h of UVA exposure.

3 Results

3.1 COA production

The cooking experiments produced substantial amounts of cooking organic aerosols (COA). The indoor mass concentrations were 177 to 282 µg m^{-3} when making pancakes, 304 to 1900 µg m^{-3} when pan-frying Brussels sprouts, and 610 to 1710 µg m^{-3} when cooking a vegetable stir-fry (Table 1). These mass concentrations were significantly above the background; the SMPS and OPS measured consistently low number concentrations prior to cooking (Fig. 1 and S10†). For example, in Fig. 1, the pan-cooking began at 75 min, producing up to 10^7 particles per cm^3 in this particular Brussels sprouts cooking event on October 4, 2021.

The total mass of COA was between 21.2 and 288 µg, and represents the upper bound of possible COA collected in the impinger (Table 1). The solutions were subsequently diluted to 50 mL, yielding a mass concentration range of 0.4 to 5.8 mg L^{-1}. We aimed to have these COA concentrations on the same order of magnitude of the concentration of organic matter in cloud water[39,42,46] as well as allow us to run photochemical experiments without significant screening of organic material.

Many variables affect the emissions of COA: the ingredients, the oil, the spices, the temperature of the pan, the air flow around the cooking experiment, and more.[3,4,47] For example, Sankhyan et al.[3] observed varying COA concentrations among different meals such as stir-fry, breakfast, chili and Thanksgiving meals prepared during the HOMEChem study,[11] highlighting the variability in COA emissions. The mass loadings we observed are also comparable with cooking activities ranging from pizzerias to Indian food stalls including dim sum and Korean BBQ.[6]

3.2 BrCOA production

The COA were collected directly into an aqueous solution by the Coriolis µ impinger, thereby avoiding any solvent extraction issues which can significantly affect the sinks of $^1O_2^*$.[18] These solutions were filtered to remove any particulates and measured using the UV/Vis spectrometer (see Methods for further details) (Fig. 2). These COA samples were light-absorbing and so we are

Table 1 The particulate mass of pre-cooking background lab aerosols and of cooking aerosols measured by the SMPS and OPS instruments. Aerosols were collected for 60 min at a flow rate of 1 L min^{-1}. Dates of sampling are in the MM/DD format (in 2021).

| Sample	Date sampled MM/DD	Pre-cooking Ave. total conc. (µg m^{-3})	Total OA collected (µg)	During cooking Ave. total conc. (µg m^{-3})	Total COA collected (µg)
Pancake	10/08	1.63	0.20	177	21.2
Pancake	10/13	2.58	0.31	282	33.8
Pancake	10/20	3.62	0.43	282	33.9
Brussels sprouts	10/04	1.18	0.14	656	78.7
Brussels sprouts	11/15	0.72	0.09	304	36.4
Brussels sprouts	11/24	2.05	0.24	1900	288
Stir-fry	10/27	2.65	0.32	610	73.2
Stir-fry	12/09	0.68	0.08	1590	191
Stir-fry	12/10	0.98	0.12	1710	205
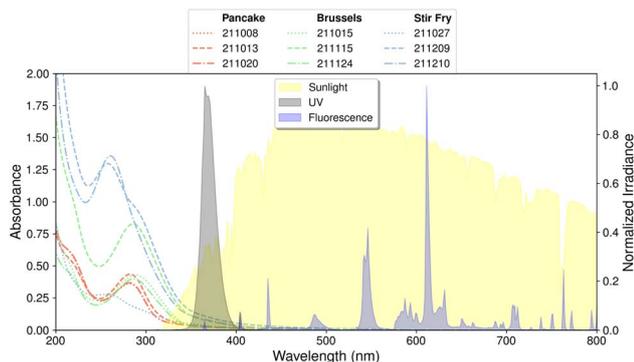
Fig. 2 The absorbance of the BrCOA are plotted as a function of wavelength and are colour-coded by dish type: pancake BrCOA (red), Brussels sprouts BrCOA (green) and stir-fry BrCOA (blue). Individual samples correspond to the date of collection in the YY-MM-DD format. The normalized irradiance of the three sources of indoor light is plotted on the right y-axis. The sunlight spectrum was measured during the window sunlit experiment on May 15, 2022. An inset of these spectra is available as Fig. S3.†

naming the chromophoric subset of COA: brown cooking organic aerosols (BrCOA). The absorbance spectra of all BrCOA showed the characteristic absorbance of BrC with a sharp absorbance peak in the near UV region (Fig. 2). Furthermore, we observed important variability in absorbance among these BrCOA samples. All three pancake BrCOA had similar absorbance and a similar peak around 280 nm, likely indicative of chromophores with similar functional groups (Fig. 2). The Brussel sprout BrCOA also had similar types of chromophores based on the absorbance profile, but at different concentrations between the cooking events. Finally, the stir-fry BrCOA had the most variability in the absolute absorbance likely since it was composed of the largest variety of ingredients (see ESI† for ingredient list) (Fig. 2).

We used three different types of indoor lights to probe the range of wavelengths available to drive indoor photochemistry: natural sunlight through a window, UVA bulbs and fluorescent tubes (Fig. 2). To quantify the overlap between the relative intensities of the three light sources depicted in Fig. 2 and the absorbance of the BrCOA samples, we next determined the rate of absorbance for each solution with each light source.

3.3 Rates of absorbance

The rate of absorbance (R_{abs}) is defined as the fraction of light absorbed by the chromophores present in each sample (eqn (4)). R_{abs} significantly depends on the emission spectra of the light source (Fig. 2). The spectral overlap is an order of magnitude less for fluorescent tubes compared to UVA and sunlight, indicating that less BrCOA molecules were excited under the fluorescent tubes (Fig. 3B). Consequently, the variability in absorbance measured from the BrCOA extracts has a negligible impact on R_{abs}. Rather, the order of magnitude of the R_{abs} value is governed by the light source. We further use the R_{abs} parameter to normalize the $^1O_2^*$ production of each sample and to calculate the apparent quantum yields of $^1O_2^*$ (see section 3.5).

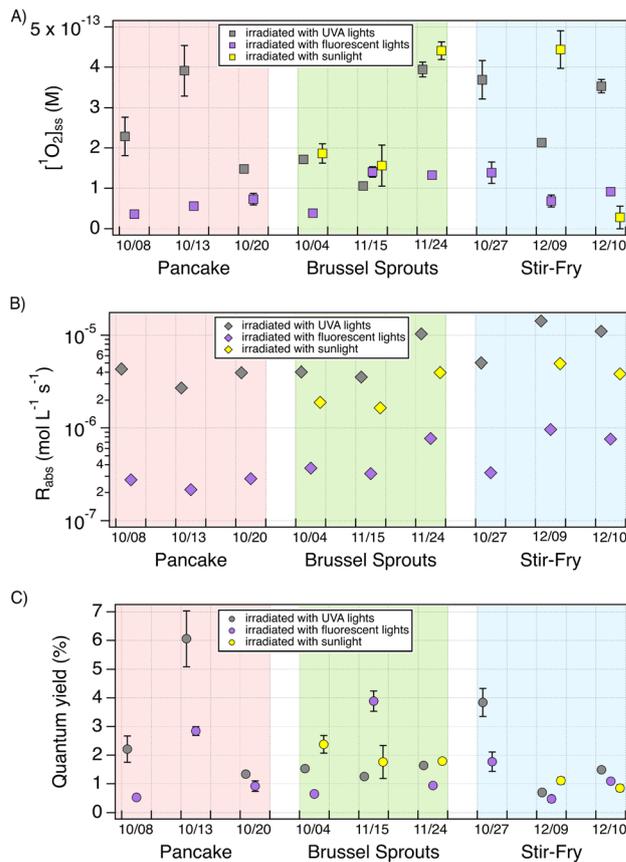Fig. 3 The singlet oxygen steady state concentrations ($[^1O_2^*]_{ss}$) (A), the rate of absorbance (R_{abs}) (B), and the apparent quantum yields (C) are plotted as a function of dish type, pancake (red), Brussels sprouts (green), stir-fry (blue) and under UVA lights (gray), fluorescent tubes (purple) and sunlight (yellow). The rate of absorbance is in the log scale. Each cooking experiment was conducted in triplicate on separate days with a new set of ingredients, and experiments were ran under the three types of lights, except for sunlight which depended on weather conditions. The error bars were calculated from the linear regression of the k_{obs} values.

3.4 $^1O_2^*$ production by BrCOA

$^1O_2^*$ production requires chromophoric species, O_2, and light, which are all present indoors. We measured $^1O_2^*$ steady state concentrations ($[^1O_2^*]_{ss}$) using FFA as a $^1O_2^*$ probe following eqn (2) (Fig. S4–S6†). Note that the background ambient aerosol solutions did not have a quantifiable FFA decay for any irradiation source, demonstrating unambiguously that the BrCOA solutions (and not the lab ambient aerosols) are responsible for the $^1O_2^*$ production (Fig. S7†). The average ($[^1O_2^*]_{ss}$) in pancake, pan-fried Brussels sprouts, and vegetable stir-fry BrCOA under UVA light were $2.56 \pm 1.24 \times 10^{-13}$ M, $2.24 \pm 1.51 \times 10^{-13}$ M and $3.12 \pm 0.86 \times 10^{-13}$ M, respectively (Fig. 3). Under fluorescent tubes, we observed $[^1O_2^*]_{ss}$ of $5.46 \pm 1.87 \times 10^{-14}$ M, $1.04 \pm 0.57 \times \times 10^{-13}$ M, and $9.96 \pm 3.58 \times 10^{-14}$ M for pancakes, Brussels sprouts, and vegetable stir-fry, respectively. Finally, under the window sunlit conditions, we observed an average $[^1O_2^*]_{ss}$ of $2.61 \pm 1.56 \times 10^{-13}$ M and $2.36 \pm 2.94 \times 10^{-13}$ M for Brussel sprouts and stir-fry, respectively. We observed higher

concentrations of $^1O_2^*$ generated under sunlight and UVA light compared to fluorescent tubes for the same COA sample (Fig. 3A).

Cooking temperature, ingredients, stirring frequency, *etc.* can have a significant impact on the food's emission factors, which frequently vary by orders of magnitude. It is therefore remarkable that all dishes and light conditions produced measurable $[^1O_2^*]_{ss}$ up to concentrations of 4.5×10^{-13} M (Fig. 3A). These $^1O_2^*$ concentrations are comparable to illuminated ambient particulate matter extracts collected in Switzerland[23,24] and in Hong Kong.[26] These concentrations are an order of magnitude lower than particulate matter collected in Davis, California.[20,48] Yet indoor $[^1O_2^*]_{ss}$ are an order of magnitude higher than PM$_{2.5}$ in Colorado.[25] Nevertheless, these values can be difficult to compare as they do not take into account different photon fluxes from different photochemical setups.

3.5 Apparent quantum yields of BrCOA

Typically, higher concentrations of chromophores would be expected to lead to higher $[^1O_2^*]_{ss}$, and thus we need to normalize to the concentrations of BrCOA in each sample. To normalize $^1O_2^*$ concentrations, we calculated the apparent quantum yield values by dividing the $[^1O_2^*]_{ss}$ by the R_{abs} according to the relative rate method using perinaphthenone as a reference sensitizer (Fig. 3).[18] Apparent quantum yield values take the absorbance-irradiation spectral overlap into account and therefore highlight best the differences in chromophoric species responsible for the $^1O_2^*$ sensitization in BrCOA (eqn (4)).

If the differences in $[^1O_2^*]_{ss}$ across BrCOA samples were solely due to differences in concentration of chromophores, then the apparent quantum yields would be identical. Indeed, the Oct 20th pancake sample, the Nov 24th Brussels sprout sample and the Dec 10th stir-fry samples have the same apparent quantum yield under fluorescent light, despite having different $[^1O_2^*]_{ss}$ (Fig. 3). In these cases, the variability in the $[^1O_2^*]_{ss}$ in Fig. 3A could be accounted for by the variability in R_{abs} in Fig. 3B, and thus by different concentrations of chromophores.

Moreover, we observed remarkably efficient $^1O_2^*$ sensitization with apparent quantum yields up to 6.1% under UVA lights for the Oct 13th pancake BrCOA (Fig. 3C). This result was driven by high $[^1O_2^*]_{ss}$ despite a low R_{abs} (Fig. 3A & B) and points to the role of low absorbing but highly efficient chromophores capable of sensitizing $^1O_2^*$. In other words, some samples have "quality" chromophores as was reported by Bogler *et al.*[24] for aged organic aerosols. Bogler *et al.*[24] reported apparent quantum yield values of PM$_{2.5}$ extracts only up to 2% over the course of a year of sampling in Switzerland. Kaur *et al.*[20] found apparent quantum yields of roughly 4% for brown carbon extracts, while surface water extract apparent quantum yields of 4% to 8% were reported by Zhou *et al.*[49] Our measurements of apparent $^1O_2^*$ quantum yields for indoor BrCOA fall within the range of previous studies.

Overall, we observe that both the "quantity" and the "quality" of chromophores present in BrCOA are important in predicting the ability of BrCOA to produce $^1O_2^*$ in lit indoor environments. The apparent quantum yields obtained confirm that the incomplete combustion of organic matter, whether from biomass burning or from cooking aerosols, are effective sensitizers of $^1O_2^*$ even under indoor lighting conditions with important implications for the oxidative potential of BrCOA.[50,51]

4 Atmospheric implications

4.1 Photochemistry of BrCOA

There is a growing body of evidence demonstrating that indoor light can initiate photochemical processes indoors, and here we show for the first time that $^1O_2^*$ can be produced indoors by irradiating chromophores present in BrC-containing cooking organic aerosols (BrCOA). The concentration and the sensitizing ability (*i.e.* the quantity and the quality) of the chromophores in BrCOA led to apparent quantum yields of $^1O_2^*$ of up to 6.1%. On average though, the values were similar to typical apparent quantum yields of 1–2% in outdoor particulate matter extracts.[24,27] Furthermore, the sources of light did not sensitize $^1O_2^*$ to the same efficiency, and indoor sunlight was the most effective in our experimental setup. Nevertheless, emitted BrCOA in a windowless environment can disperse in a kitchen environment, especially under poor ventilation, leading to BrCOA interacting with indoor light fixtures either above a stove or on the ceiling. Understanding the effect of the light source and its distance from an emitted plume of BrCOA is warranted.

The production of $^1O_2^*$ confirms indirectly the production of excited triplet state organics within BrCOA.[52] We are therefore proposing that two additional types of oxidants, namely $^1O_2^*$ and by extension excited triplet state organics, are present indoors and can participate in oxidizing BrCOA under lit indoor environments. We expect that $^1O_2^*$ is contributing to BrCOA aging, and to oxidation state increases observed for example by Takhar *et al.*[53] From cooking oils alone, there is the potential of generating reactive oxygen species within BrCOA, likely from unsaturated aldehydes as precursors to peroxides.[54] This result can be extended to our study where we used olive oil and sunflower oil, as we expect unsaturated aldehydes to absorb at higher wavelengths due to their conjugated π-system. Furthermore, the presence of quinones in BrCOA could also be partly responsible for the observed $^1O_2^*$ sensitization.[50,51,55] Quinones are oxidation products of naphthalene,[56] and were observed previously in SOA by Manfrin *et al.*[23] to produce $^1O_2^*$ in apparent quantum yields up to 11%.

4.2 Sustained $[^1O_2^*]_{ss}$ as a competitive oxidant in indoor environments

In this study, we aimed to capture the most variability in our $^1O_2^*$ sensitization experiments by reproducing each dish-specific cooking experiment on three separate days with ingredients purchased on different days (ingredients and recipes are detailed in the ESI†). In other words, we purposefully created maximum variability in our experiments to understand when and why $^1O_2^*$ would be produced.

We report concentrations of $[^1O_2^*]_{ss}$ on the order of 10^{-13} M. These concentrations represent 3 orders of magnitude higher concentrations than OH radicals.[23] However, OH radicals have

© 2024 The Author(s). Published by the Royal Society of Chemistry

Environ. Sci.: Atmos., 2024, **4**, 611–619 | **617**

rate constants with common organic molecules which are 3 orders of magnitude more reactive than $^1O_2^*$.[23] Thus, $^1O_2^*$ can be a competitive reactive oxygen species.

Furthermore, the sunlit experiments indicate that $[^1O_2^*]_{ss}$ can be sustained for over 40 min of irradiation (Fig. S6†). These steady-state concentrations suggest that the production of $^1O_2^*$ is not occurring as a burst of oxidant, which has been observed for OH radicals for example by Paulson et al.,[57] but rather as a sustained production of $^1O_2^*$ over time. This sustained $[^1O_2^*]_{ss}$ could then lead to $^1O_2^*$ having a prolonged ability to oxidize indoor aerosols and impact air quality.

4.3 Indoor air quality

There is also growing evidence that exposure to ultrafine particles from cooking are linked to adverse health effects.[58,59] Laursen et al.[60] observed oxidatively damaged DNA in blood after exposure to COA, but only observed a weak association between short-term exposure to emissions from cooking to inflammation in individuals with mild asthma. Recommendations for reducing exposure to cooking aerosols would include increased ventilation and air filtration,[61] particularly since many residents are unaware of the benefits of ventilation.[62] The cooking method can have an impact on the number and mass concentrations of emitted BrCOA. For instance, a domestic air fryer produced up to 5 times more PM_{10} than pan cooking, which can lead to more BrCOA.[63] Overall, presence of $^1O_2^*$ in indoor environments opens questions about the fate, transformations and lifetime of $^1O_2^*$ in the built environment.

Author contributions

NBD designed the research. MMJ and RL ran the cooking experiments. MMJ collected the UV/Vis and $^1O_2^*$ data. NBD, KG and CS developed the data analysis procedure. NBD and KG analysed and plotted the UV/Vis and $^1O_2^*$ data. RL collected and analysed the SMPS and OPS data. NBD and SZ developed the cooking experimental setup and the impinger collection method. NBD and KG wrote the manuscript with contributions from RL, MMJ and CS.

Conflicts of interest

There are no conflicts to declare.

Acknowledgements

Notes and references

1 A. Laskin, J. Laskin and S. A. Nizkorodov, Chem. Rev., 2015, 115, 4335.

2 R. F. Hems, E. G. Schnitzler, C. Liu-Kang, C. D. Cappa and J. P. Abbatt, ACS Earth Space Chem., 2021, 5, 722–748.

3 S. Sankhyan, S. Patel, E. F. Katz, P. F. DeCarlo, D. K. Farmer, W. W. Nazaroff and M. E. Vance, Environ. Sci.: Processes Impacts, 2021, 23, 1476–1487.

4 S. Sankhyan, K. Zabinski, R. E. O'Brien, S. Coyan, S. Patel and M. E. Vance, Environ. Sci.: Atmos., 2022, 2, 1364–1375.

5 C. Mohr, P. F. DeCarlo, M. F. Heringa, R. Chirico, J. G. Slowik, R. Richter, C. Reche, A. Alastuey, X. Querol, R. Seco, J. Peñuelas, J. L. Jiménez, M. Crippa, R. Zimmermann, U. Baltensperger and A. S. H. Prévôt, Atmos. Chem. Phys., 2012, 12, 1649–1665.

6 X. Zhao, Q. Hu, X. Wang, X. Ding, Q. He, Z. Zhang, R. Shen, S. Lü, T. Liu, X. Fu and L. Chen, J. Atmos. Chem., 2015, 72, 1–18.

7 Y. Omelekhina, A. Eriksson, F. Canonaco, A. S. H. Prevot, P. Nilsson, C. Isaxon, J. Pagels and A. Wierzbicka, Environ. Sci.: Processes Impacts, 2020, 22, 1382–1396.

8 M. Takhar, Y. Li, J. C. Ditto and A. W. H. Chan, Environ. Sci.: Processes Impacts, 2023, 25, 165–175.

9 M. Crippa, P. F. DeCarlo, J. G. Slowik, C. Mohr, M. F. Heringa, R. Chirico, L. Poulain, F. Freutel, J. Sciare, J. Cozic, C. F. Di Marco, M. Elsasser, J. B. Nicolas, N. Marchand, E. Abidi, A. Wiedensohler, F. Drewnick, J. Schneider, S. Borrmann, E. Nemitz, R. Zimmermann, J.-L. Jaffrezo, A. S. H. Prévôt and U. Baltensperger, Atmos. Chem. Phys., 2013, 13, 961–981.

10 Y. Zhu, Q. Wang, X. Yang, N. Yang and X. Wang, Atmosphere, 2021, 12, 892.

11 D. K. Farmer, M. E. Vance, J. P. D. Abbatt, A. Abeleira, M. R. Alves, C. Arata, E. Boedicker, S. Bourne, F. Cardoso-Saldaña, R. Corsi, P. F. DeCarlo, A. H. Goldstein, V. H. Grassian, L. H. Ruiz, J. L. Jimenez, T. F. Kahan, E. F. Katz, J. M. Mattila, W. W. Nazaroff, A. Novoselac, R. E. O'Brien, V. W. Or, S. Patel, S. Sankhyan, P. S. Stevens, Y. Tian, M. Wade, C. Wang, S. Zhou and Y. Zhou, Environ. Sci.: Processes Impacts, 2019, 21, 1280–1300.

12 Y. B. Lim, Y. Tan, M. J. Perri, S. P. Seitzinger and B. J. Turpin, Atmos. Chem. Phys., 2010, 10, 10521–10539.

13 B. Ervens, B. J. Turpin and R. J. Weber, Atmos. Chem. Phys., 2011, 11, 11069–11102.

14 T. Fang, P. S. J. Lakey, R. J. Weber and M. Shiraiwa, Environ. Sci. Technol., 2019, 53, 12784–12792.

15 H. Tong, P. S. J. Lakey, A. M. Arangio, J. Socorro, F. Shen, K. Lucas, W. H. Brune, U. Pöschl and M. Shiraiwa, Environ. Sci. Technol., 2018, 52, 11642–11651.

16 A. M. Arangio, H. Tong, J. Socorro, U. Pöschl and M. Shiraiwa, Atmos. Chem. Phys., 2016, 16, 13105–13119.

17 S. Wang, Y. Zhao, A. W. H. Chan, M. Yao, Z. Chen and J. P. D. Abbatt, Chem. Rev., 2023, 123, 1635–1679.

18 R. Ossola, O. M. Jönsson, K. Moor and K. McNeill, Chem. Rev., 2021, 121, 4100–4146.

19 B. C. Faust and J. M. Allen, J. Geophys. Res.: Atmos., 1992, 97, 12913–12926.

20 R. Kaur, J. R. Labins, S. S. Helbock, W. Jiang, K. J. Bein, Q. Zhang and C. Anastasio, Atmos. Chem. Phys., 2019, 19, 6579.

21 R. Kaur and C. Anastasio, Atmos. Environ., 2017, 164, 387–397.

22 R. Kaur and C. Anastasio, *Environ. Sci. Technol.*, 2018, **52**, 5218.

23 A. Manfrin, S. Nizkorodov, K. Malecha, G. Getzinger, K. McNeill and N. Borduas-Dedekind, *Environ. Sci. Technol.*, 2019, **53**, 8553–8562.

24 S. Bogler, K. R. Daellenbach, D. M. Bell, A. S. H. Prévôt, I. El Haddad and N. Borduas-Dedekind, *Environ. Sci. Technol.*, 2022, **56**, 15389–15397.

25 F. Leresche, J. R. Salazar, D. J. Pfotenhauer, M. P. Hannigan, B. J. Majestic and F. L. Rosario-Ortiz, *Environ. Sci. Technol.*, 2021, **55**, 13152–13163.

26 Y. Lyu, Y. H. Lam, Y. Li, N. Borduas-Dedekind and T. Nah, *Atmos. Chem. Phys.*, 2023, **23**, 9245–9263.

27 L. Ma, R. Worland, L. Heinlein, C. Guzman, W. Jiang, C. Niedek, K. J. Bein, Q. Zhang and C. Anastasio, *Atmos. Chem. Phys.*, 2024, **24**, 1–21.

28 S. Zhou, S. F. Kowal, A. R. Cregan and T. F. Kahan, *Indoor Air*, 2021, **31**, 1187–1198.

29 C. J. Young, S. Zhou, J. A. Siegel and T. F. Kahan, *Environ. Sci.: Processes Impacts*, 2019, **21**, 1229–1239.

30 A. Gandolfo, V. Gligorovski, V. Bartolomei, S. Tlili, E. Gómez Alvarez, H. Wortham, J. Kleffmann and S. Gligorovski, *Build. Environ.*, 2016, **109**, 50–57.

31 S. F. Kowal, S. R. Allen and T. F. Kahan, *Environ. Sci. Technol.*, 2017, **51**, 10423–10430.

32 J. Liu, H. Deng, P. S. J. Lakey, H. Jiang, M. Mekic, X. Wang, M. Shiraiwa and S. Gligorovski, *Environ. Sci. Technol.*, 2020, **54**, 15680–15688.

33 E. Gómez Alvarez, D. Amedro, C. Afif, S. Gligorovski, C. Schoemaecker, C. Fittschen, J.-F. Doussin and H. Wortham, *Proc. Natl. Acad. Sci. U. S. A.*, 2013, **110**, 13294–13299.

34 S. Patel, S. Sankhyan, E. K. Boedicker, P. F. DeCarlo, D. K. Farmer, A. H. Goldstein, E. F. Katz, W. W. Nazaroff, Y. Tian, J. Vanhanen and M. E. Vance, *Environ. Sci. Technol.*, 2020, **54**, 7107–7116.

35 S. Patel, D. Rim, S. Sankhyan, A. Novoselac and M. E. Vance, *Environ. Sci.: Processes Impacts*, 2021, **23**, 1706–1717.

36 H. L. Davies, C. O'Leary, T. Dillon, D. R. Shaw, M. Shaw, A. Mehra, G. Phillips and N. Carslaw, *Environ. Sci.: Processes Impacts*, 2023, **25**, 1532–1548.

37 W. L. F. Armarego and C. Chai, *Purification of Laboratory Chemicals*, Butterworth-Heinemann, Boston, 7th edn, 2013, pp. 103–554.

38 M. Gómez-Domenech, H. García-Mozo, P. Alcázar, R. Brandao, E. Caeiro, V. Munhoz and C. Galán, *Aerobiologia*, 2010, **26**, 149–155.

39 S. Müller, C. Giorio and N. Borduas-Dedekind, *ACS Environ. Au*, 2023, **3**, 164–178.

40 E. F. Katz, H. Guo, P. Campuzano-Jost, D. A. Day, W. L. Brown, E. Boedicker, M. Pothier, D. M. Lunderberg, S. Patel, K. Patel, P. L. Hayes, A. Avery, L. Hildebrandt Ruiz, A. H. Goldstein, M. E. Vance, D. K. Farmer, J. L. Jimenez and P. F. DeCarlo, *Aerosol Sci. Technol.*, 2021, **55**, 1099–1114.

41 J. R. Laszakovits, S. M. Berg, B. G. Anderson, J. E. O'Brien, K. H. Wammer and C. M. Sharpless, *Environ. Sci. Technol. Lett.*, 2017, **4**, 11–14.

42 N. Borduas-Dedekind, R. Ossola, R. O. David, L. S. Boynton, V. Weichlinger, Z. A. Kanji and K. McNeill, *Atmos. Chem. Phys.*, 2019, **19**, 12397–12412.

43 W. R. Haag, J. Hoigné, E. Gassman and A. Braun, *Chemosphere*, 1984, **13**, 631–640.

44 E. Appiani, R. Ossola, D. E. Latch, P. R. Erickson and K. McNeill, *Environ. Sci.: Processes Impacts*, 2017, **19**, 507–516.

45 R. Schmidt, C. Tanielian, R. Dunsbach and C. Wolff, *J. Photochem. Photobiol., A*, 1994, **79**, 11–17.

46 R. D. Cook, Y.-H. Lin, Z. Peng, E. Boone, R. K. Chu, J. E. Dukett, M. J. Gunsch, W. Zhang, N. Tolic, A. Laskin and K. A. Pratt, *Atmos. Chem. Phys.*, 2017, **17**, 15167.

47 S. Wang, M. Takhar, Y. Zhao, L. N. S. Al Rashdi and A. W. H. Chan, *ACS Earth Space Chem.*, 2021, **5**, 1150–1162.

48 W. Jiang, L. Ma, C. Niedek, C. Anastasio and Q. Zhang, *ACS Earth Space Chem.*, 2023, **7**, 1107–1119.

49 H. Zhou, S. Yan, L. Lian and W. Song, *Environ. Sci. Technol.*, 2019, **53**, 2482–2490.

50 Y. Yang, M. A. Battaglia, E. S. Robinson, P. F. DeCarlo, K. C. Edwards, T. Fang, S. Kapur, M. Shiraiwa, M. Cesler-Maloney, W. R. Simpson, J. R. Campbell, A. Nenes, J. Mao and R. J. Weber, *ACS ES&T Air*, 2024, **1**, 188–199.

51 Y. Liu and C. K. Chan, *Environ. Sci.: Processes Impacts*, 2022, **24**, 525–546.

52 K. McNeill and S. Canonica, *Environ. Sci.: Processes Impacts*, 2016, **18**, 1381.

53 M. Takhar, Y. Li and A. W. H. Chan, *Atmos. Chem. Phys.*, 2021, **21**, 5137–5149.

54 S. Wang, P. J. Gallimore, C. Liu-Kang, K. Yeung, S. J. Campbell, B. Utinger, T. Liu, H. Peng, M. Kalberer, A. W. Chan and J. P. Abbatt, *Environ. Sci. Technol.*, 2023, **57**, 1246–1256.

55 L. Gerritz, M. Schervish, P. S. J. Lakey, T. Oeij, J. Wei, S. A. Nizkorodov and M. Shiraiwa, *J. Phys. Chem. A*, 2023, **127**, 5209–5221.

56 R. D. McWhinney, S. Zhou and J. P. D. Abbatt, *Atmos. Chem. Phys.*, 2013, **13**, 9731–9744.

57 S. E. Paulson, P. J. Gallimore, X. M. Kuang, J. R. Chen, M. Kalberer and D. H. Gonzalez, *Sci. Adv.*, 2019, **5**, eaav7689.

58 L. A. Wallace, H. Mitchell, G. T. O'Connor, L. Neas, M. Lippmann, M. Kattan, J. Koenig, J. W. Stout, B. J. Vaughn, D. Wallace, M. Walter, K. Adams, L.-J. S. Liu and Inner-City Asthma Study, *Environ. Health Perspect.*, 2003, **111**, 1265–1272.

59 L. Wallace and W. Ott, *J. Exposure Sci. Environ. Epidemiol.*, 2011, **21**, 20–30.

60 K. R. Laursen, N. V. Christensen, F. A. Mulder, J. Schullehner, H. J. Hoffmann, A. Jensen, P. Møller, S. Loft, A.-C. Olin, B. B. Rasmussen, B. Rosati, B. Strandberg, M. Glasius, M. Bilde, T. Sigsgaard and The Climate Chamber Group, *Part. Fibre Toxicol.*, 2023, **20**, 26.

61 J. Li, G. Fan, Y. Ou and Q. Deng, *Energy Build.*, 2023, **294**, 113232.

62 L. Sun and B. C. Singer, *J. Exposure Sci. Environ. Epidemiol.*, 2023, **33**, 439–447.

63 X. Wang and A. W. H. Chan, *Environ. Sci. Technol.*, 2023, **57**, 17384–17392.

© 2024 The Author(s). Published by the Royal Society of Chemistry

Environ. Sci.: Atmos., 2024, **4**, 611–619 | **619**